International Journal of Solids and Structures 45 (2008) 5856–5866

Contents lists available at ScienceDirect

International Journal of Solids and Structures

journal homepage: www.elsevier.com/locate/ijsolstr

Mesoscopic modeling of Acoustic Emission through an energetic approach

Federico Bosia [a,*], Nicola Pugno [b], Giuseppe Lacidogna [b], Alberto Carpinteri [b]

[a] Department of Physics, Politecnico di Torino, Corso Duca degli Abruzzi 24, 10124 Torino, Italy
[b] Department of Structural Engineering and Geotechnics, Politecnico di Torino, Torino, Italy

ARTICLE INFO

Article history:
Received 14 February 2008
Received in revised form 17 May 2008
Available online 4 July 2008

Keywords:
Acoustic Emission
Algorithms
Concrete
Fracture
Energy balance
Fracture
Modelling
Numerical methods

ABSTRACT

The aim of the present work is to present a simple model for damage progression and Acoustic Emission that correctly accounts for energy dissipation due to the formation of micro-cracks and the creation of surfaces in a material undergoing external loading, and thus to derive the scaling behaviour observed in experiments. To do this, energy balance considerations are included in a Fibre Bundle Model approach. The model predictions are first illustrated in a uniaxial test under quasistatic loading conditions. Numerical results are then compared to experimental data relative to tests on masonry elements of various sizes subjected compression. The scaling properties of Acoustic Emission under the chosen energy balance assumptions is analyzed and compared to previous numerical and experimental results in the literature. Power-law scaling behaviour is found with respect to specimen dimensions.

© 2008 Elsevier Ltd. All rights reserved.

1. Introduction

Acoustic emission (AE) is the term commonly used to indicate the stress waves produced by the sudden internal stress redistribution caused by the changes in the internal structure of a material subjected to loading (Carpinteri and Lacidogna, 2007). There are a number of possible causes for the internal-structure changes, both reversible and irreversible: crack initiation and growth, crack opening and closure, dislocation movements etc. In composite materials, other mechanism are also present, like fibre breakage and fibre-matrix debonding. Most of the sources of AE are damage-related; thus, the detection and monitoring of these emissions are commonly used to predict material failure. However, AE deriving from reversible modifications in material structure, e.g. material rearrangements, or fracture followed by healing processes (White et al., 2001), are also possible.

Various attempts have been made in the literature to describe the qualitative and quantitative behaviour emerging in AE experiments. Typically, instead of using a continuum-mechanics approach, simple mass-spring models have been adopted, whereby an AE event is associated with a sudden spring stiffness variation (e.g. in Pollock, 1973). Another widely used approach is that employed in so-called Fibre-Bundle Models (FBM), both discrete and continuous (Turcotte et al., 2003; Kun et al., 2000; Hidalgo et al., 2001). These models have allowed to simulate correct constitutive laws, damage clustering, AE energy bursts, etc. in various cases. Two-dimensional scalar lattice models for microfracturing have also been introduced, to numerically simulate the advancement of cracks and the resulting AE activity, including estimations of avalanche sizes and power-law behaviour (Zapperi et al., 1997; Minozzi et al., 2003). In all of these approaches, however, essential aspects of fracture mechanics, such as energy dissipation and fracture energy balance, are often neglected (see e.g. Caldarelli et al.,

* Corresponding author. Tel.: +39 116707889;fax: +39 6707214.
E-mail address: fbosia@to.infn.it (F. Bosia).

0020-7683/$ - see front matter © 2008 Elsevier Ltd. All rights reserved.
doi:10.1016/j.ijsolstr.2008.06.019

1996; Pradhan and Hemmer, 2008). In addition, the description of AE as a critical phenomenon is often oversimplified without resorting to well-established fracture mechanics concepts as the energy release rate of a material.

Recent analysis of AE experiments has highlighted the multiscale aspect of cracking and damaging phenomena (Carpinteri and Pugno, 2005): when one considers the dissipative processes occurring over the sample volume, it is possible to show that energy dissipation takes place over a fractal domain, which is comprised between euclidean surfaces and volumes. This is because in AE experiments, as in all damaging processes, a part of the mechanical energy stored in the deforming material is dissipated due to crack formation and propagation. Fractal statistical analysis has thus been applied by some of the authors to analyse and describe experimental data (Carpinteri et al., 2004a; Carpinteri et al., 2004b; Carpinteri et al., 2006). Based on this, experimental analysis has been extended to the scaling of AE activity with specimen size, which apart from its theoretical interest, provides a valuable tool to estimate component lifetime.

In this contribution, the aim is to introduce energy balance considerations into a simple damage model based on a FBM approach, and compare the resulting AE scaling behaviour with that found in the literature. Additionally, simulations are used to confirm previous experimental results by the authors showing power law scaling of AE energy with respect to specimen dimensions.

The model is described in Section 2, typical results in the specific case of a thin bar subjected to a uniaxial load are presented in Section 3, and a comparison between numerical predictions and experimental results in the case of masonry volumes of various sizes is discussed in Section 4. The conclusions and outlook are provided in Section 5.

2. Model

To correctly describe the phenomenon of AE occurring in quasistatic loading experiments, our goal is to introduce the simplest possible model containing the correct energetic behaviour. For the sake of simplicity, we use a FBM approach (Smith and Phoenix, 1981; Harlow and Phoenix, 1978; Bazant and Pang, 2006), applied to a specimen having length L and cross-section A. In this approach, the specimen is modelled as a "chain of bundles", i.e. a discrete arrangement of $N_x \times N_y$ fibres (or springs), as shown in Fig. 1. Each spring is identified by the index pair (i,j), with $i = 1 \ldots N_x$ and $j = 1 \ldots N_y$. The specimen is thus discretized in N_x portions, each modelled as an array (or "bundle") of N_y parallel springs. Two opposite uniaxial forces of time-varying magnitude $F(t)$ are applied at the two ends of the specimen, each undergoing a displacement of magnitude $x(t)$ in the direction of the force.

In the simplest possible approach, all springs are considered identical in length l and in elastic parameters (Young's modulus E), but their cross-section A_{ij} is allowed to vary (with uniform probability) within chosen limits, i.e. $A_{min} < A_{ij} < A_{max}$, with the total specimen cross section remaining constant. This introduces some statistical variation in the released AE energies, as observed experimentally. The stiffness of a single spring can therefore be written as $k_{ij} = EA_{ij}/l$, whilst the equivalent stiffness of the i-th undamaged material portion, represented by the i-th arrangement of $N_y(i)$ parallel springs, is

$$K_i = \sum_{j=1}^{N_y(i)} k_{ij} \tag{1}$$

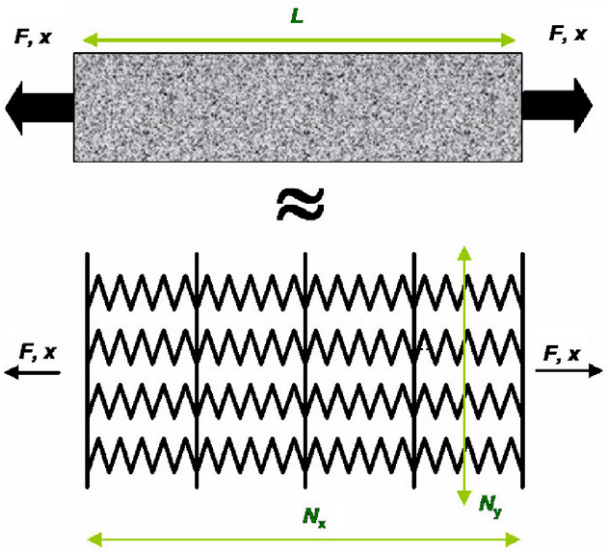

Fig. 1. Discretization of a specimen of length L subjected to a uniaxial force F (generating an elongation x) by means of a N_x by N_y spring arrangement (in the figure, $N_x = N_y = 4$).

The length and cross-section of the entire specimen are, respectively:

$$L = \sum_{i=1}^{N_x} l_i = N_x l, \quad A = \sum_{j=1}^{N_y(i)} A_{ij} (\forall i) \tag{2}$$

Next, a fracture criterion is introduced whereby the failure of the individual spring (i,j) occurs when it undergoes a stress σ_{ij} that exceeds its intrinsic strength σ_{Cij}. The value of σ_{Cij} is assumed to vary from spring to spring and to be distributed randomly, according to the Weibull distribution (Hermann and Roux, 1990), which is widely used in fracture mechanics. The probability distribution $P(\sigma_{Cij})$ of the spring strengths can therefore be expressed as:

$$P(\sigma_{Cij}) = 1 - e^{\left[-\left(\frac{\sigma_{Cij}}{\sigma_C}\right)^m\right]} \tag{3}$$

where σ_C is a nominal stress value for the material under investigation, and m is the Weibull modulus, which is characteristic of the considered material. An AE event is modelled as the failure of a single spring used to discretize the specimen. In the case of failure of the (i,j)-th spring, its stiffness k_{ij} is set equal to zero, and the load is redistributed uniformly among the remaining springs in the i-th bundle. This is known in the literature as an "Equal Load Sharing (ELS)" FBM (Pradhan and Hansen, 2005). It is clear that, as the loading of the specimen increases and the resulting damaging process advances, the stiffness of each section of the material will decrease as fewer and fewer springs forming the section remain intact. Therefore, the stiffness of each section is time dependent, i.e. $K_i = K_i(t)$. Correspondingly, the overall specimen stiffness $K(t)$ decreases in time. The overall specimen stiffness variation $\Delta K_{ij}(t)$ (or compliance variation $\Delta C_{ij}(t)$) deriving from a single AE event occurring at the location (i,j) depends on its location and on time, as is intuitive. Detailed calculations are given in Appendix A.

The energetic aspects of AE events are now considered. Energy balance considerations require that the variation of the total potential energy $\Delta U_{ij}(t)$, when an AE event occurs, be compensated by the kinetic energy $\Delta T_{ij}(t)$ released in the form of a stress wave generated in the sample. The energetic contribution of the dissipated energy $\Delta\Omega_{ij}(t)$ in the formation of a crack surface at micro- or meso-scale must also be considered. Thus, one can write:

$$\Delta U_{ij}(t) + \Delta T_{ij}(t) + \Delta\Omega_{ij}(t) = 0 \tag{4}$$

In Force-Controlled (FC) or Displacement-Controlled (DC) quasistatic experiments the elastic potential energy variation for the failure of a single (i,j) spring, corresponding to an AE event, can be written as, respectively:

$$(FC)\ \Delta U_{ij}(t) = -\frac{1}{2} F(t)^2 \Delta C_{ij}(t) \tag{5}$$

$$(DC)\ \Delta W_{ij}(t) = \frac{1}{2} x(t)^2 \Delta K_{ij}(t) \tag{6}$$

The dissipated energy $\Delta\Omega_{ij}$ is assumed to be proportional to the newly created surface A_{ij}:

$$\Delta\Omega_{ij} = G_C A_{ij} \tag{7}$$

where G_C is the critical strain energy release rate of the material. All the above energy contributions can be expressed as a function of the accumulated elastic energy of the (i,j)-th spring at failure when the AE event takes place (see appendix A):

$$\Phi_{ij} = \frac{1}{2} \frac{\sigma_{Cij}^2}{E} A_{ij} l \tag{8}$$

In the chosen ELS approximation, the kinetic energy released in AE can be written, according to the previous equations, as:

$$\Delta T_{ij}(t) = (\eta_i(t) - \gamma_{ij}) \Phi_{ij} \tag{9}$$

where:

$$\gamma_{ij} = \frac{2EG_C}{\sigma_{Cij}^2 l} \tag{10}$$

and

$$\eta_{ij}^{FC}(t) = \frac{K_i(t)}{K_i(t) - k_{ij}};\ (FC) \tag{11}$$

$$\eta_{ij}^{DC}(t) = \frac{K(t')}{K(t)} \frac{K_i(t)}{K_i(t) - k_{ij}}\ (DC) \tag{12}$$

where t' and t are the instants immediately before and after the AE event, respectively. In numerical simulations, where time discretization is employed, $t' = t + 1$. The dissipated energy can also be expressed by means of the accumulated energy in the (i,j)-th spring:

$$\Delta\Omega_{ij} = \gamma_{ij} \Phi_{ij} \tag{13}$$

Thus, ΔT_{ij} and $\Delta\Omega_{ij}$ are both proportional to Φ_{ij} (and therefore proportional to one another) as well as complementary, i.e. their sum equals the total elastic energy variation. The other quantities of interest in simulations are the external work ΔL_{ij}:

$$\Delta L_{ij} = 2\eta_{ij}(t)\Phi_{ij} \tag{14}$$

and the accumulated elastic energy in the whole structure $\Delta\Psi_{ij}(t)$:

$$\Delta\Psi_{ij} = \eta_{ij}(t)\Phi_{ij} \tag{15}$$

It is worth pointing out that $\Delta L_{ij} = 2\Delta\Psi_{ij}$, in accordance with Clapeyron's theorem.

3. Numerical results and AE scaling

As first example, a specimen is considered in the form of a thin bar of length $L = 10^{-2}$m and cross section $A = 10^{-6}$m^2, discretized by means of a $N_x = 100$, $N_y = 1000$ spring arrangement. The material constants are typical for concrete, with Young's modulus $E = 23$ GPa, peak stress $\sigma_C = 10$ MPa, and Weibull modulus m varying between 0.5 and 6. As, explained above, material heterogeneity is modelled by randomly assigning spring cross sections A_{ij} in simulations, with the constraint that the specimen cross section remains constant ($\sum_j A_{ij} = A, \forall i$). The specimen is subjected to traction with a displacement x increasing linearly in time: $x = vt$.

At first, the numerically obtained scaling properties for number of AE events and for released AE energy are compared. The number of AE events, indicated here with N_{AE}, correspond simply to the number of springs undergoing failure when their intrinsic strength is exceeded, whilst the released kinetic energy T accounts for energy dissipation, and is therefore expected to display a different scaling behaviour.

Fig. 2a shows stress-strain results for a typical numerical experiment with $m = 3$ and the chosen specimen discretization. The curve is typical for brittle fracture, and displays only some softening before failure occurs. To obtain ductile behaviour a refinement of the model would be required, including a correct description the crack tip field, shielding effects of plastic deformation on the crack growth, etc. (Rice and Tracey, 1969; Beltz et al., 1999). This modification is beyond the scope of this work. However, for practical purposes, the phenomenology of ductile behaviour can also be obtained using the present approach by choosing wide Weibull distributions for σ_{Cij} (i.e. small m values) and small N_x values. This is the case in Fig. 2b, for $m = 0.9$ and $N_x = 5$ where a softening phase is present before failure.

Typically, in the case of a linearly increasing load and brittle fracture, the number of AE events N_{AE} increases with power law behaviour with time up to failure, as do the released kinetic energy T, the dissipated energy Ω, the external work W and the accumulated elastic energy in the structure ψ. In this case, it is possible to fit the experimental data with $N_{AE} \propto t^{\alpha}$, $T \propto t^{\beta}$ where α and β are non-integer exponents that are strongly dependent on the chosen Weibull modulus m. The simulated behaviour for T in the case of the above specimen is shown in Fig. 3. Numerical predictions can be compared to experimental data (e.g. in Carpinteri et al., 2004b.), and a best fit on the data allows the determination of the most appropriate Weibull modulus value for the material under study. In the case of Carpinteri et al., 2004b., $m \approx 3$, which gives $\alpha = 3.0 \pm 0.2$ and $\beta = 5.4 \pm 0.2$.

The main goal of the model is to verify the predicted scaling behaviour with specimen dimensions (length, cross-section, and volume) and compare it with experimental results in the literature. It was shown in experiments by some of the authors (Carpinteri and Pugno, 2005; Carpinteri et al., 2004a; Carpinteri et al., 2004b) that the number of AE events scales with non-integer exponents smaller than unity, indicating that AE occurs in a fractal domain with dimensions comprised between

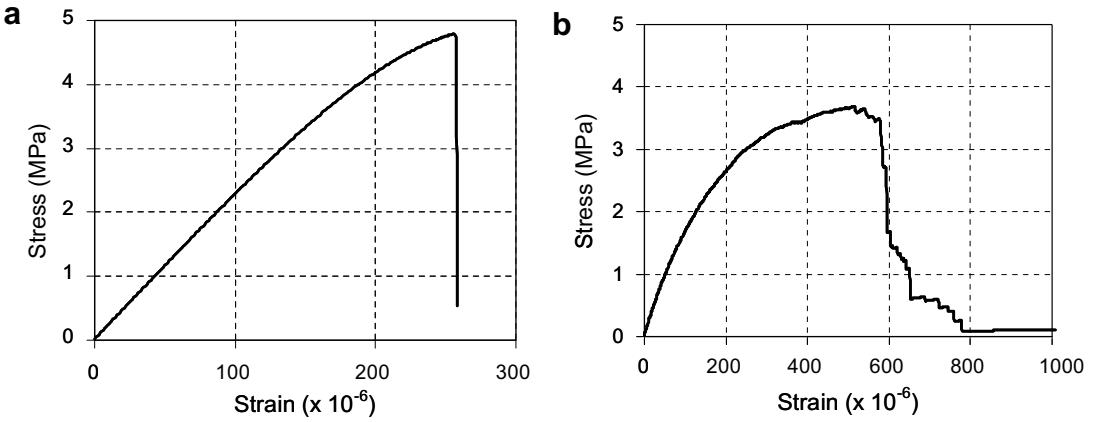

Fig. 2. Stress-strain curve for a model specimen subjected to traction up to failure in displacement-controlled simulations: a) brittle fracture; b) ductile fracture.

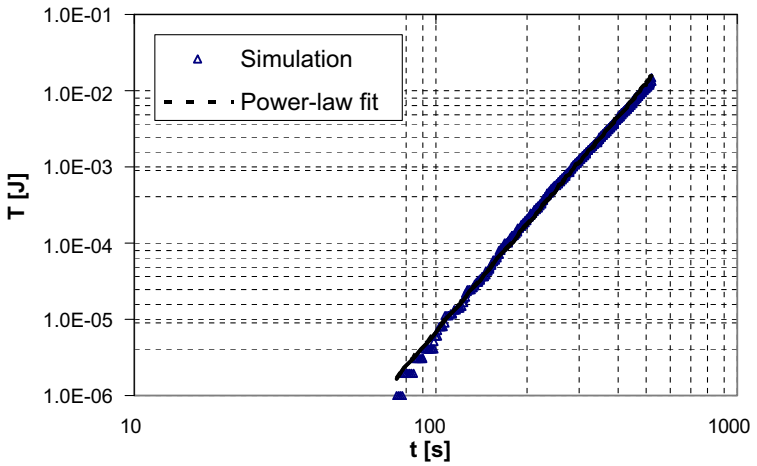

Fig. 3. Power-law growth in the released AE kinetic energy T vs. time t for a simulation with a linearly increasing imposed displacement.

those of a surface and those of a volume. Thus, the objective is to verify the congruence of the numerical results obtained with the present model with experimental scaling laws, and to determine their exponents, namely:

$$a)\ N_{AE} \propto L^{d_{N_1}}\ \ b)\ N_{AE} \propto A^{d_{N_2}}\ \ c)\ N_{AE} \propto V^{d_{N_3}} \tag{16}$$

for the number of AE events and

$$a)\ T \propto L^{d_{T_1}}\ \ b)\ T \propto A^{d_{T_2}}\ \ c)\ T \propto V^{d_{T_3}} \tag{17}$$

for their kinetics.

To do this, specimens of different dimensions are considered in the simulations, and N_{AE} and T are calculated at specimen failure. In particular, the specimen length L is varied between 10^{-6} m and 10^{-2} m (with corresponding discretizations N_x varying between 1 and 10^4) and the cross-section A is varied between 10^{-10} m^2 and 10^{-4} m^2 (with corresponding discretizations N_y varying between 1 and 10^3).

As a uniaxial tensile test is considered, the loading direction x is expected to be the relevant dimension with respect to which non-integer scaling occurs. Indeed, the exponents d_{N2}, d_{N3}, d_{T2}, d_{T3} are all on average close to unity after repeated simulations, indicating direct proportionality and trivial scaling behaviour, as expected. On the other hand, simulations for different specimen lengths produce average values of $d_{N1} = 0.8 \pm 0.1$ and $d_{T1} = 0.6 \pm 0.1$, respectively. Both exponents are consistent with the experimentally derived effect of non-integer scaling, however the latter of the two differs considerably from unity, indicating that the released kinetic energy in AE is a variable which displays a greater divergence of from direct proportionality. This could be due to the fact that when considering T instead of N_{AE}, the dissipated energy is accounted for, as explained in Section 2. Fig. 4 displays typical results for the T vs. L dependence. The data points are averages deriving from repeated numerical simulations, with the error bars representing their standard deviation. It is clear that the afore-mentioned power-law fit adequately fits the data, whilst a linear fit (also included for comparison purposes) does not.

Another point of interest is to verify the predicted distribution of AE events in each burst (i.e. occurring at each loading step) and the corresponding AE energy distribution. Analytical and numerical results for FBMs in the literature (Hemmer and Hansen, 1992) indicate that the relative occurrence of events in a burst follows a power law with universal exponent $-5/2$. Smaller exponent values are found in particular cases when specific hypotheses are added (e.g. Hidalgo et al., 2001), for example by introducing a lower cutoff in the fibre failure stress distribution (Pradhan and Hansen, 2005). The same behaviour is found in the case of the present model, with and average exponent value of -2.3 ± 0.2, depending on the chosen Weibull distribution in fibre strengths. The small discrepancy with the $-5/2$ value can probably be attributed to the limited size of the chosen sample.

More importantly, it is of interest to analyze the distribution of the released AE energies ΔT in bursts. Asymptotic results for equal load sharing FBMs are shown in the literature to follow the same law as for the number of broken bonds, i.e. a power law with exponent $-5/2$ (Pradhan and Hemmer, 2008). Experimental results in the literature also show that the distribution is a power law (Diodati et al., 1991; Cannelli et al., 1993; Petri et al., 1994), in analogy with the Gutenberg- Richter law in seismology (Richter, 1958). This is considered to be indicative of an underlying critical dynamics, confirming the absence of a characteristic length and the self-similarity of the microfracturing phenomenon. The expected behaviour is thus of the form:

$$P(\Delta T) \propto \Delta T^{-\lambda} \tag{18}$$

where $P(\Delta T)$ is the number of AE events with a released kinetic greater than ΔT. However, contrary to numerical results, experimental data indicate that typical values for the scaling exponent for the considered materials are close to the value $\lambda = 1.3$.

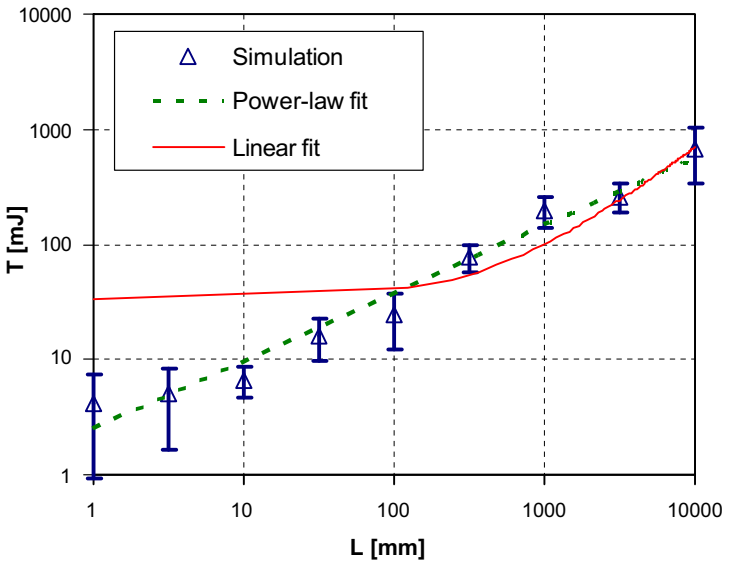

Fig. 4. Numerically computed scaling properties of AE energy T vs. specimen length L. Linear and power law fits are included. Error bars derive from the standard deviation of results from repeated simulations.

Typical simulation data using the present model are reported in Fig. 5 in log-log scale, together with a fit based on Eq. (18). The fit correctly describes the data, except for a slight deviation in the large energy range, as in Pradhan and Hemmer, 2008. The value of the exponent for the data shown is $\lambda = 1.9 \pm 0.1$, though values may vary between 1.6-2.1, depending on the chosen specimen discretization and Weibull fibre strength distribution. It is interesting to notice that these values are closer to the mentioned experimental results than FBM numerical approaches in the literature, despite the simplicity of the present approach. Similar exponent values are also found in other numerical studies using lattice models (e.g. Caldarelli et al., 1996).

The relationship between the released AE energy T and the number of AE events N_{AE} for each burst as well as for a typical simulation are shown in Fig. 6a and b, respectively. The function $T(N_{AE})$ increases monotonically with power law behaviour and exponents typically ranging between 1 and 3, depending on the chosen parameters. This behaviour is qualitatively similar to that found experimentally by some of the authors in previous experimental tests (Carpinteri et al., 2006).

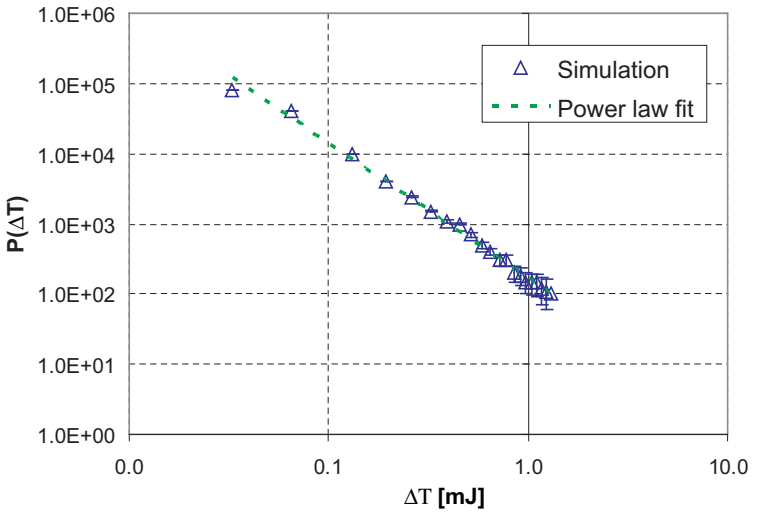

Fig. 5. Typical simulated AE burst energy distribution.

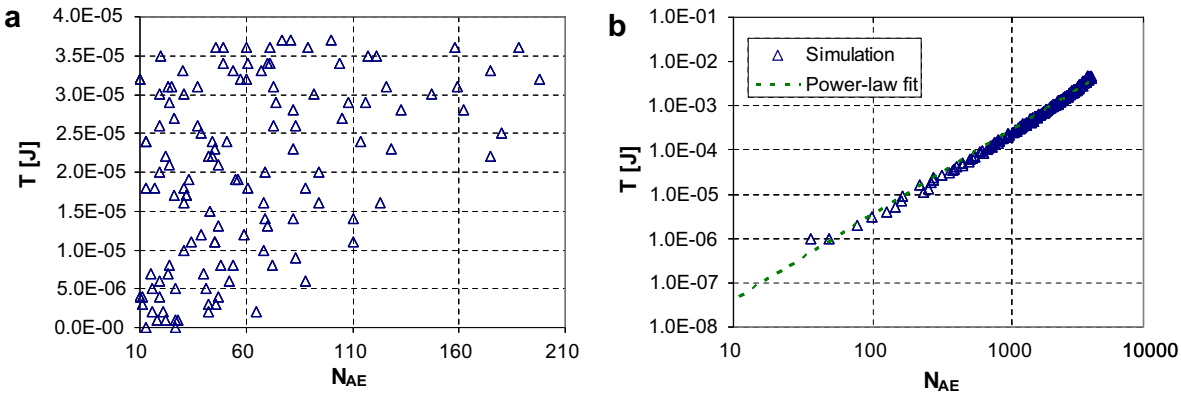

Fig. 6. AE energy T vs. number of AE events N_{AE} for a) single bursts, b) an entire simulation. Both are in log-log scale and are fitted with a power law.

4. Modelling of a compressive test on masonry elements

Next, model predictions are compared to experimental AE data deriving from tests on specimens of different dimensions, so that size scaling issues can be addressed. The chosen specimens are three masonry specimens having different lengths and the same cross section, and quasistatic testing is carried out in compression.

4.1. Experimental

The measurements are conducted on the specimens through the combined use of double jacks and AE sensors (Carpinteri and Lacidogna, 2007). The prismatic masonry volumes tested in compression are shown in Fig. 7. Their lengths are L_1 = 300 mm, L_2 = 590 mm, L_3 = 1180 mm, respectively, and their width and breadth are w = 240, b = 120 mm. The bricks are 60 mm wide, and the mortar layers are 10 mm thick. The dimensions of the cross-section of the elements correspond to the effective area of the masonry to which the pressure of the flat-jacks is applied. The tests comply with standard procedures specified in ASTM (1991b), apart from the vertical cuts produced in order to eliminate, in the damaged element, the influence of the adjacent masonry portions.

Various loading cycles are applied with increasing stress levels, as shown in Fig. 8, during which the cumulative number of AE events N_{AE} is monitored. For each test, the maximum number of AE events N_{max} at peak-stress σ_{max} is recorded. Results are summarized in Table 1 and further discussed in the next section, together with those deriving from simulations.

4.2. Simulations

The three specimens are modelled with the approach described in Section 2 and simulations are carried out with known material constants: Young's modulus E = 20 GPa, mean peak stress in compression σ_C = 5 MPa, and critical strain energy re-

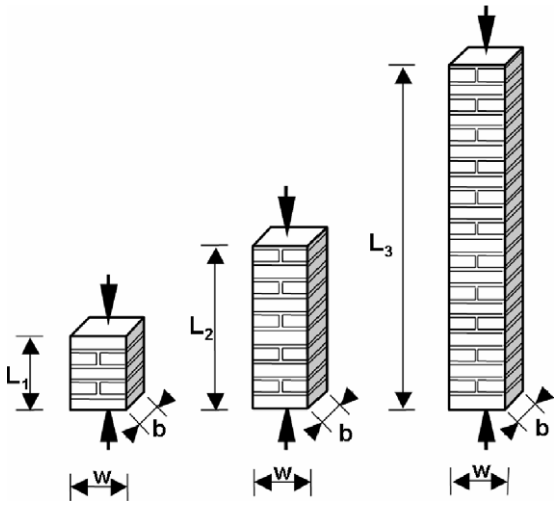

Fig. 7. Three masonry specimens tested in compression (arrows indicate loading direction).

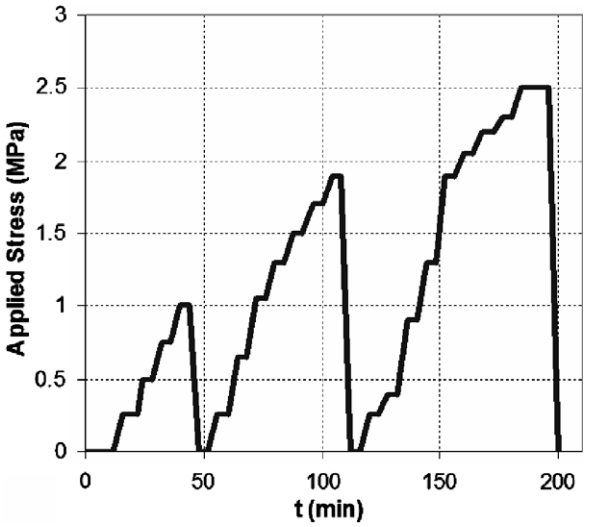

Fig. 8. Adopted loading protocol in tests on masonry elements.

Table 1
Experimental values obtained from flat-jack tests and AE measurements

Specimen	V (m^3)	σ_{max} (MPa)	N_{max}
1	0.8640	2.07	6500
2	1.6992	1.61	12000
3	3.3984	1.59	18000

lease rate $G_C = 10$ J/m^2. The chosen discretization is $N_x = 5000$ and $N_y = 1000$. The experimental loading protocol, shown in Fig. 8, is applied in the simulations and the resulting failure stress σ_{max} and cumulative number of AE events N_{max} is recorded and compared to that obtained experimentally in each case.

Good agreement is obtained in the three cases using Weibull modulus values comprised between 1.5 and 2. Results for are shown for N_{AE} vs. t in Fig. 9 for the intermediate specimen ($L_2 = 590$ mm). The plot shows that AE takes place when the stress level reached previously is exceeded (thus highlighting Kaiser effect), a result obtained both experimentally and in

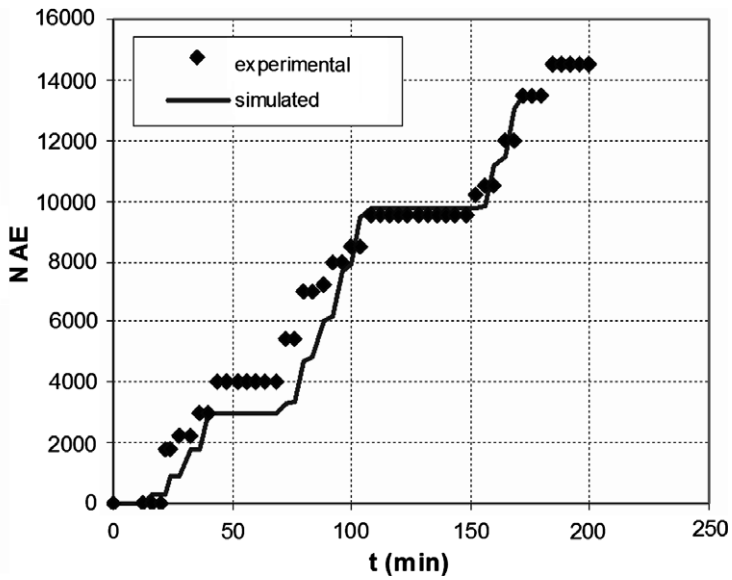

Fig. 9. Simulated and experimentally derived N_{AE} vs. time for specimen n.2, using the loading protocol shown in Fig. 8.

simulations. Experimental and numerical results are compared both in terms of peak stress σ_{max} and number of AE events vs. time. An appropriate choice of parameters yields similar peak stress values and a similar time evolution in the AE activity produced in the sample, apart from statistical variations due to randomly distributed spring strengths in the simulations (Fig. 9). Once determined, these parameters are used in the following to study the AE scaling behaviour.

Again, the interest lies in analysing the predicted scaling behaviour by varying specimen dimensions and comparing it with experimental results, to verify that AE occurs in a fractal domain with dimensions comprised between those of a surface and those of a volume. The assumed relation is:

$$N_{AE}(V) \propto V^{D/3} \tag{19}$$

where D is comprised between 2 and 3. Introducing the fractal acoustic emission density Γ_{AE}, one can write:

$$\Gamma_{\mathrm{AE}} = N_{\max}/V^{D/3} \tag{20}$$

where N_{max} is the maximum number of AE events, evaluated at peak-stress.

The experimental results summarized in Table 1 show that the cumulative number of AE events increases nonlinearly with increasing specimen volume. By best-fitting of the results of these tests, a value of $D/3 \cong 0.7$ is obtained, so that the fractal exponent, as predicted by fragmentation theories, turns out to be $D \cong 2.1$, and the critical value of fractal AE density $\Gamma_{AE} \cong 8.00\ \mathrm{cm}^{-2.2}$.

Numerical simulation results for scaling of N_{AE} vs. specimen volume V yield D values typically comprised between 2.5 and 3, i.e. values above those obtained experimentally. Those for T vs. V, instead, give rise to similar D values to experimental ones. These data are shown in Fig. 10, with linear and power law fits included for comparison. It is clear that the linear fit is inadequate, whilst the power law fit yields and exponent $D \cong 2.1 \pm 0.1$, in accordance with the experimental value. This experimental-numerical comparison confirms the validity of the adopted approach, based on energy balance considerations.

5. Conclusions

In conclusion, a simple phenomenological model has been presented that can capture a number of important characteristics that emerge in damage progression experiments and AE measurements. In particular, using a correct energetic formulation of fracture events in the model, whereby part of the stored elastic energy is released in the creation of surfaces at micro/mesoscopic level, leads to numerical confirmation of experimental results for the AE energy power law scaling behaviour with respect to specimen volume in the case of compression tests on masonry specimens. Apart from the theoretical interest related to these scaling issues, the proposed modelization can serve as a useful tool to numerically evaluate energetic aspects of AE, even when this has not been done experimentally. This can be important, for example, when carrying out b-value analysis (Colombo et al., 2003) to predict failure in structures.

Having verified the general reliability of the model, additional developments will be the object of further work, e.g. an extension of the model to 2-D or 3-D, an extension of the analysis to a "Local load-sharing" FBM model (i.e. the removal of the mean-field stress approximation), or the introduction of nonlinear or hysteretic behaviour in the springs. Thus, it should be possible to investigate more complex experimental situations, to detect variations in AE scaling behaviour and critical exponents during various phases of damage progression, to study AE event clustering and localization, or other aspects, e.g. to correlate nonlinear or hysteretic behaviour to AE.

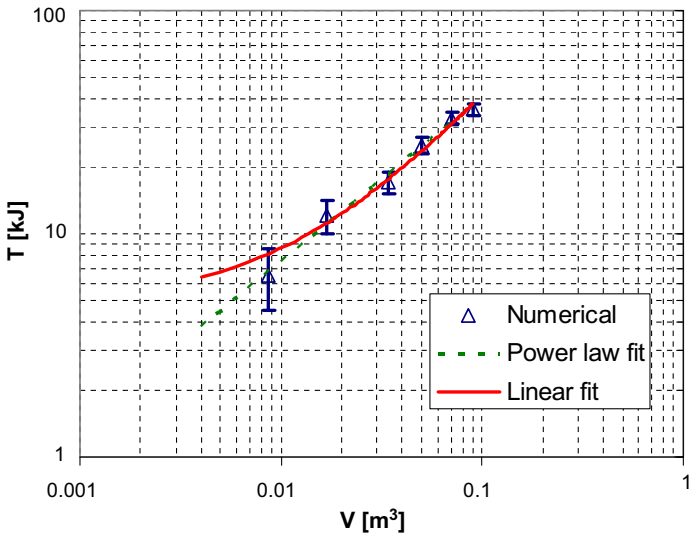

Fig. 10. Simulated released AE energy vs. specimen volume (log-log scale). Linear and power-law fits are included for comparison.

Acknowledgements

The authors wish to thank Dr. M. Scalerandi and Dr. A.S. Gliozzi (Politecnico di Torino) for fruitful discussions.

Appendix A. There follows a complete derivation of the formulas given in Section 2 and used in the model described in this paper. As mentioned in Section 2, the stiffness of the i-th spring bundle in the arrangement shown in Fig. 1 can be written as:

$$K_i(t) = \sum_{j=1}^{N_y(t)} k_{ij} \tag{A.1}$$

where $N_y(t)$ is the number of undamaged fibres for the i-th bundle at time t and $k_{ij} = EA_{ij}/l$ is the stiffness of a single fibre, which is set to zero when the fibre fails, when $\sigma_{ij}(t) > \sigma_{Cij}$. The corresponding overall compliance variation $\Delta C_{ij}(t)$ of the chain of bundles constituting the specimen when a single fibre at location (i,j) fails can then be written as

$$\begin{aligned}&\Delta C_{ij}(t) = \\ &= \frac{1}{K_1(t)} + \cdots + \frac{1}{K_i(t) - k_{ij}} + \cdots \frac{1}{K_{Nx}(t)} - \frac{1}{K_1(t)} \cdots - \frac{1}{K_i(t)} \cdots - \frac{1}{K_{Nx}(t)} = \frac{1}{K_i(t) - k_{ij}} - \frac{1}{K_i(t)} \\ &= \frac{K_i(t) - K_i(t) + k_{ij}}{K_i(t)(K_i(t) - k_{ij})} = \frac{k_{ij}}{K_i(t)(K_i(t) - k_{ij})}\end{aligned} \tag{A.2}$$

whilst the stiffness variation corresponding to the same AE event is:

$$\Delta K_{ij} = \frac{1}{C(t')} - \frac{1}{C(t)} = \frac{C(t) - C(t')}{C(t')C(t)} = -\frac{\Delta C_{ij}}{C(t')C(t)} = -\Delta C_{ij} K(t') K(t) = -\frac{K(t')K(t)k_{ij}}{K_i(t)(K_i(t) - k_{ij})} \tag{A.3}$$

where t' and t are the instants immediately before and after the AE event, respectively.

In **Force Control (FC)** the released kinetic energy for a single AE event can be written as:

$$\Delta T_i(t) = -\Delta W_i(t) - \Delta \Omega_i = \frac{1}{2} F^2 \Delta C_{ij}(t) - G_C A_i \tag{A.4}$$

Denoting with F_{ij} and x_{ij} the force and the displacement relative to the (i,j)-th spring, F_{Bi} and x_{Bi} the force and the displacement relative to the i-th bundle, respectively, and considering the series/parallel spring configuration of the bundles and-springs (see Fig. 1), we have:

$$F_{ij} = k_{ij} x_{ij} = k_{ij} x_{Bi} \Rightarrow x_{Bi} = \frac{F_{ij}}{k_{ij}} \tag{A.5}$$

and

$$Kx = F = F_{Bi} = x_{Bi} K_i \Rightarrow F = F_{ij} \frac{K_i}{k_{ij}} \tag{A.6}$$

where the time dependence has been omitted for brevity. Eq. (A.4) becomes:

$$\Delta T_i = \frac{1}{2} \left(F_{ij} \frac{K_i}{k_{ij}} \right)^2 \frac{k_{ij}}{K_i(K_i - k_{ij})} - G_C A_i = \frac{1}{2} \frac{F_{ij}^2 K_i}{k_{ij}(K_i - k_{ij})} - G_C A_i = \Phi_{ij} \left(\frac{K_i}{K_i - k_{ij}} - \frac{2EG_C}{\sigma_{Cij}^2 l} \right) = (\eta_{ij} - \gamma_{ij}) \Phi_{ij} \tag{A.7}$$

where

$$\Phi_{ij} = \frac{1}{2} \frac{F_{ij}^2}{k_{ij}} \bigg|_{atfailure} = \frac{1}{2} \frac{\sigma_{Cij}^2}{E} \quad \eta_{ij}^{FC} = \frac{K_i - k_{ij}}{K_i} \quad \gamma_{ij} = \frac{2EG_C}{\sigma_{Cij}^2 l} \tag{A.8}$$

In **Displacement Control (DC)** we have:

$$\Delta T_i(t) = -\Delta W_i(t) - \Delta \Omega_i = \frac{1}{2} x^2 \Delta K_{ij}(t) - G_C A_i \tag{A.9}$$

so that

$$\Delta T_i = \frac{1}{2} \left(F_{ij} \frac{K_i}{K(t) k_{ij}} \right)^2 \frac{K(t') K(t) k_{ij}}{K_i(K_i - k_{ij})} - G_C A_i = \frac{1}{2} \frac{F_{ij}^2 K_i K(t')}{k_{ij} K(t)(K_i - k_{ij})} - G_C A_i = \Phi_{ij} \left(\frac{K(t') K_i}{K(t)(K_i - k_{ij})} - \frac{2EG_C}{\sigma_{Cij}^2 l} \right) = (\eta_{ij} - \gamma_{ij}) \Phi_{ij} \tag{A.10}$$

where

$$\eta_{ij}^{DC}(t) = \frac{K(t')}{K(t)} \frac{K_i(t)}{K_i(t) - k_{ij}} \tag{A.11}$$

References

ASTM Standard Test Method for Determining the Mechanical Properties of Hardened Concrete Under Triaxial Loads. (1991b).

Bazant, Z.P., Pang, S., 2006. Mechanics-based statistics of failure risk of quasibrittle structures and size effect on safety factors. Proceedings of the National Academy of Sciences 103, 9434.

Beltz, G.E., Lipkin, D.M., Fischer, L.L., 1999. Role of Crack Blunting in Ductile Versus Brittle Response of Crystalline Materials. Physical Review Letters 82 (22), 4468–4471.

Caldarelli, G., Di Tolla, F.D., Petri, A., 1996. Self-Organization and Annealed Disorder in a Fracturing Process. Physical Review Letters 77 (12), 2503–2506.

Cannelli, G., Cantelli, R., Cordero, F., 1993. Self-organized criticality of the fracture processes associated with hydrogen precipitation in niobium by acoustic emission. Physical Review Letters 70, 3923.

Carpinteri, A., Lacidogna, G. (Eds.), 2007. Earthquakes and Acoustic Emission: Selected Papers from the 11th International Conference on Fracture, Turin, Italy, March 20-25, 2005. Taylor & Francis, London.

Carpinteri, A., Lacidogna, G., Pugno, N., 2004a. A Fractal Approach for Damage Detection in concrete and Masonry Structures by the Acoustic Emission Technique. Acoustique et Techniques 38, 31–37.

Carpinteri, A., Lacidogna, G., Pugno, N., 2004b. Damage diagnosis and life-time assessment of concrete and masonry structures by an acoustic emission technique. In: V.C. Li et al. (Eds.), Fracture Mechanics of Concrete and Concrete Structures: Proceedings of the 5th International FraMCoS Conference, vol. 1, pp. 31- 40.

Carpinteri, A., Pugno, N., 2005. Are Scaling Laws on Strength of Solids Related to Mechanics or to Geometry? Nature Materials 4 (6), 421–423.

Carpinteri, A., Lacidogna, G., Pugno, N., 2006. Richter's laws at the laboratory scale interpreted by acoustic emission. Magazine of Concrete Research 58 (9), 619–625.

Carpinteri, A., Lacidogna, G., 2007. Damage evaluation of three masonry towers by acoustic emission. Engineering Structures 29 (7), 1569–1579.

Colombo, I.S., Main, I.G., Ford, M.C., 2003. Assessing damage of reinforced concrete beam using b-value analysis of acoustic emission signal. Journal of Materials in Civil Engineering 15, 280–286.

Diodati, P., Marchesoni, F., Piazza, S., 1991. Acoustic emission from volcanic rocks: An example of self-organized criticality. Physical Review Letters 67, 2239.

Harlow, D.G., Phoenix, S.L., 1978. The chain-of bundles probability model for the strength of fibrous materials I & II. Journal of Composite Materials 12, 195.

Hemmer, P.C., Hansen, A., 1992. The distribution of simultaneous fiber failures in fiber bundles. Journal of Applied Mechanics 59, 909.

Hermann, H.J., Roux, S., 1990. Modelization of fracture in disordered systems. In: Hermann, H.J., Roux, S. (Eds.), Statistical models for the fracture of disordered media. Elsevier Science Publishers, North Holland.

Hidalgo, R.C., Kun, F., Hermann, H.J., 2001. Bursts in a fiber bundle model with continuous damage. Physical Review E 64, 066122.

Kun, F., Zapperi, S., Hermann, H.J., 2000. Damage in Fiber Bundle Models. European Physical Journal B 17, 269–279.

Minozzi, M., Caldarelli, G., Pietronero, L., Zapperi, S., 2003. Dynamic fracture model for acoustic emission. European Physical Journal B 36, 203–207.

Petri, A., Paparo, G., Vespignani, A., Alippi, A., Costantini, M., 1994. Experimental evidence for Critical Dynamics in Microfracturing Processes. Physical Review Letters 73 (25), 3423–3426.

Pollock, A.A., 1973. Acoustic emission amplitudes. Non-destructive Testing 6 (5), 264–269.

Pradhan, S., Hansen, A., 2005. Failure properties of loaded fiber bundles having a lower cutoff in fiber threshold distribution. Physical Review E 72, 026111.

Pradhan, S., Hemmer, P.C., 2008. Energy bursts in fiber bundle models of composite materials. Physical Review E 77, 031138.

Rice, J.R., Tracey, D.M., 1969. On the ductile enlargement of voids in triaxial stress fields. Journal of the Mechanics of Solids 17, 201–217.

Richter, C.F., 1958. Elementary Seismology. W.H. Freeman and Company, S. Francisco and London.

Smith, R.L., Phoenix, S.L., 1981. Asymptotic distributions for the failure of fibrous materials under series-parallel structure and equal load-sharing. ASME Journal of Applied Mechanics 48, 75.

Turcotte, D.L., Newman, W.I., Shcherbakov, R., 2003. Micro and macroscopic models of rock fracture. Geophysical Journal International 152, 718–728.

White, S.R. et al, 2001. Autonomic healing of polymer composites. Nature 409, 794–797.

Zapperi, S., Vespignani, A., Stanley, H.E., 1997. Plasticity and avalanche behaviour in microfracturing phenomena. Nature 338, 658–660.